ARL-TR-9469 ● JUNE 2022

DEVCOM ARMY RESEARCH LABORATORY

The Influence of Soil Air-Void Fraction and Water Content on Momentum Transfer from Explosive Charges Buried in a Lean Clay

by Collin R Pecora, William L Fourney, Ulrich H Leiste, Leslie C Taylor, and David M Fox

NOTICES

Disclaimers

The findings in this report are not to be construed as an official Department of the Army position unless so designated by other authorized documents.

Citation of manufacturer's or trade names does not constitute an official endorsement or approval of the use thereof.

Destroy this report when it is no longer needed. Do not return it to the originator.

ARL-TR-9469 ● JUNE 2022

The Influence of Soil Air-Void Fraction and Water Content on Momentum Transfer from Explosive Charges Buried in a Lean Clay

Collin R Pecora and David M Fox
DEVCOM Army Research Laboratory

William L Fourney, Ulrich H Leiste, and Leslie C Taylor
University of Maryland, College Park

REPORT DOCUMENTATION PAGE

Form Approved
OMB No. 0704-0188

1. REPORT DATE *(DD-MM-YYYY)*	2. REPORT TYPE	3. DATES COVERED (From - To)
June 2022	Technical Report	7 August 2021 – 31 May 2022

4. TITLE AND SUBTITLE
The Influence of Soil Air-Void Fraction and Water Content on Momentum Transfer from Explosive Charges Buried in a Lean Clay

5a. CONTRACT NUMBER

5b. GRANT NUMBER

5c. PROGRAM ELEMENT NUMBER

6. AUTHOR(S)
Collin R Pecora, William L Fourney, Ulrich H Leiste, Leslie C Taylor, and David M Fox

5d. PROJECT NUMBER

5e. TASK NUMBER

5f. WORK UNIT NUMBER

7. PERFORMING ORGANIZATION NAME(S) AND ADDRESS(ES)
DEVCOM Army Research Laboratory
ATTN: FCDD-RLW-TG
Aberdeen Proving Ground, MD 21005

8. PERFORMING ORGANIZATION REPORT NUMBER
ARL-TR-9469

9. SPONSORING/MONITORING AGENCY NAME(S) AND ADDRESS(ES)

10. SPONSOR/MONITOR'S ACRONYM(S)

11. SPONSOR/MONITOR'S REPORT NUMBER(S)

12. DISTRIBUTION/AVAILABILITY STATEMENT
Approved for public release: distribution unlimited.

13. SUPPLEMENTARY NOTES

14. ABSTRACT
A series of experiments were conducted to quantify impulsive response of flat target plates subjected to detonation of explosive charges shallowly buried in a lean clay. The aim of this research is to correlate impulse delivered as a function of predetonative soil state derived from a three-phase soil model. Primary focus is on impulsive response as a function of the soil's air-volume fraction and water content, but other soil state parameters are explored. This work used scaled mine-blast experiments where target mass, target presented area, charge mass, charge aspect ratio, soil type, depth of burial, and energetic source to target distance were held constant while only the soil's water content and the amount of compaction effort used to construct the soil bed were varied. The results show a strong correlation between impulse delivered and air-volume fraction, and for a given air-volume fraction, greater impulse is delivered for soil with higher water content.

15. SUBJECT TERMS
buried blast, mine blast, soil state, impulse, air-void content, Terminal Effects

16. SECURITY CLASSIFICATION OF:			17. LIMITATION OF ABSTRACT	18. NUMBER OF PAGES	19a. NAME OF RESPONSIBLE PERSON
a. REPORT	b. ABSTRACT	c. THIS PAGE			Collin R Pecora
Unclassified	Unclassified	Unclassified	UU	42	19b. TELEPHONE NUMBER (Include area code) (410) 278-6153

Contents

List of Figures

List of Tables

1. Introduction

Full-scale blast experiments are costly; small-scale experimental methods can be used to gain insight into the interactions between solid structures and the mechanical energy produced by buried explosives. The problems of the response of continua and structures to excitation by relatively shallow[1,2] and deeply buried explosives[3,4] have been studied for many years.

Various problems, including crater formation,[5] ground shock propagation,[6,7] vehicle mine blast loading,[7] damage to underwater structures,[8] treatment of the blast field produced by submerged explosives,[9] and underwater channeling,[10] have contributed to the research in this area.

From the context of thermochemical energy of detonation, plate throwing is an energy-inefficient process, as targets with finite dimensions only receive a small fraction of the available energy of detonation. Even with the inefficiency, there are significant performance differences between plate throwing in free air blast and plate throwing from shallow buried blast.

If we denote the impulse delivered to a plate at a fixed plate-to-charge distance from the fraction of the energy of detonation the plate receives in air to be 1, we predict the impulse delivered in the surface laid condition to be approximately 2. Shallow buried charges produce impulse values between 3 and 18 depending on the state of the soil surrounding the charge. This increase in transmitted impulse in the buried condition relative to air blast are due to the following:

1) Additional impulse from soil particulates impacting the target.

2) Smaller product gas volumes at comparable states. For instance, in the buried condition, the specific volume of the product gases at the time when the volume has expanded to be in contact with the target is on the order of 10% of the total product gas volume and therefore at significantly higher thermodynamic pressures.

3) Velocity gradient of the impulse (dynamic) pressure at comparable states. The shape of the product gas volume at first contact with the target in the buried condition is generally nonspherical and biased toward the target, thus increasing the magnitude of the loading.

Fox and Lee[11] performed computations for target loading from explosive buried in dry sand, partially saturated sand, and water, and compared the results with those from experimental results reported by Fourney et al.[12] For both computation and experiment, loading increased with increasing water content and decreased with

increasing air-volume fraction. Westine[7] and Fourney et al.[12] used scaling laws to compare buried-blast results from different datasets without any prescribed variation of soil properties.

Recent work was performed by Fox et al.[13] using 4.4-g explosive charges either submerged in water or buried in each of three noncohesive soil types: 1) a Unified Soil Classification System[14] (USCS) clayey sand (SC), 2) a poorly graded sand (SP), or 3) a silty sand (SM). The work showed that while soil properties like mass density, compressibility, soil–water content, and strength of the medium surrounding the explosive could be correlated to peak momentum transferred to a structure, the single soil-state parameter that provided the strongest correlation was the air-volume fraction of the soil surrounding the explosive. A plot of impulse delivered versus air-volume fraction from Fox et al.[13] as well as computational results from Fourney et al.[15] is reproduced in Fig. 1.

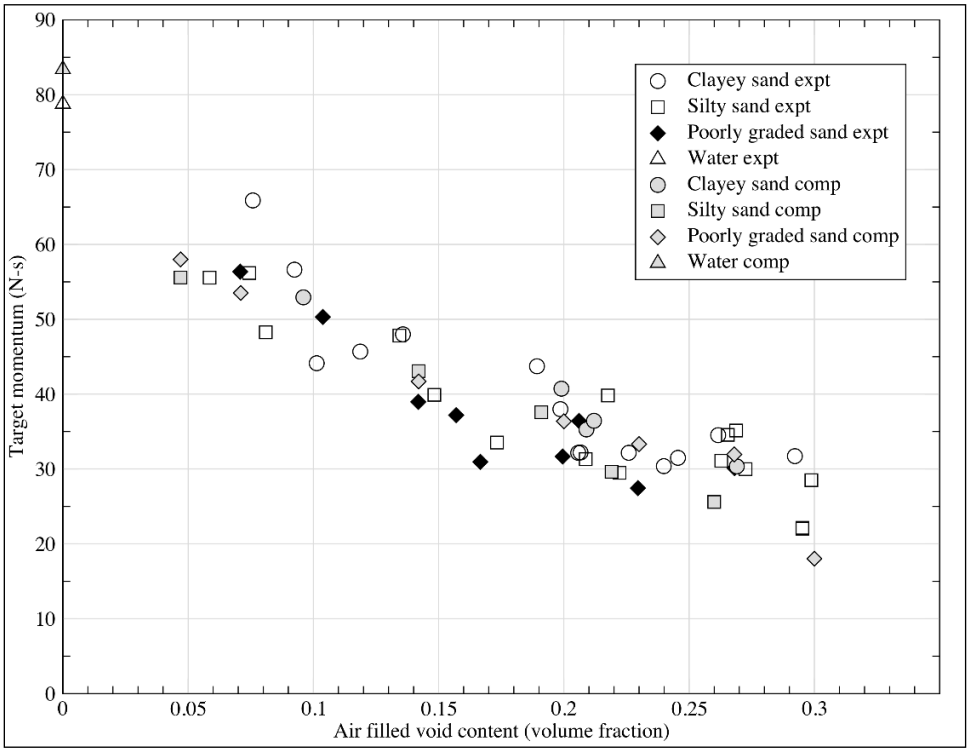

Fig. 1 Impulse vs. air-volume fraction for noncohesive soils and water

Air-volume fraction is the volumetric measure of the air content in a three-phase soil model and is inversely proportional to the energy lost compacting the soil to its fully saturated and/or compacted state, hence the inverse relationship between impulse and air-volume fraction shown in Fig. 1.

One observation from Fox et al.[13] is that USCS classification alone is not sufficient to differentiate impulsive response between soils and that soil engineering parameters such as particle-size distribution, liquid limit, and plasticity index, for example, only determine how easily, in a compaction effort sense, a soil will reach a particular air-volume fraction.

In a three-phase soil model, air-volume fraction is a linear combination of solid-volume fraction and water-volume fraction, indicating that the same air-volume fraction can be achieved by differing the volumetric ratio of the water and solid phases. The volumetric ratio of water to solid-volume fraction reduces to wG_s.The current work examines the effects of a series of constant air-volume fractions obtained at various levels of moisture content on the momentum transferred to flat target plates from explosives that are buried in a lean clay, referred throughout this manuscript as Red Lean Clay, classified as a CL type soil under USCS. The soil is more cohesive in its behavior than the soils examined previously by Fox et al.[13] The soil's particle size distribution is shown in Fig. 2 along with the three soils used in Fox et al.[13]

Three target gravimetric water contents (w) were chosen: low (w = 0.087), medium (w = 0.119), and high (w = 0.153). Additionally, three target air-volume fractions were also chosen: low (α_a = 0.0120), medium (α_a = 0.180), and high (α_a = 0.232). The water contents and air-volume fraction values were chosen to span operational soil states and are supported by available computational soil models. The target air-volume fraction values were later extended to span values between approximately 0.05 and 0.45.

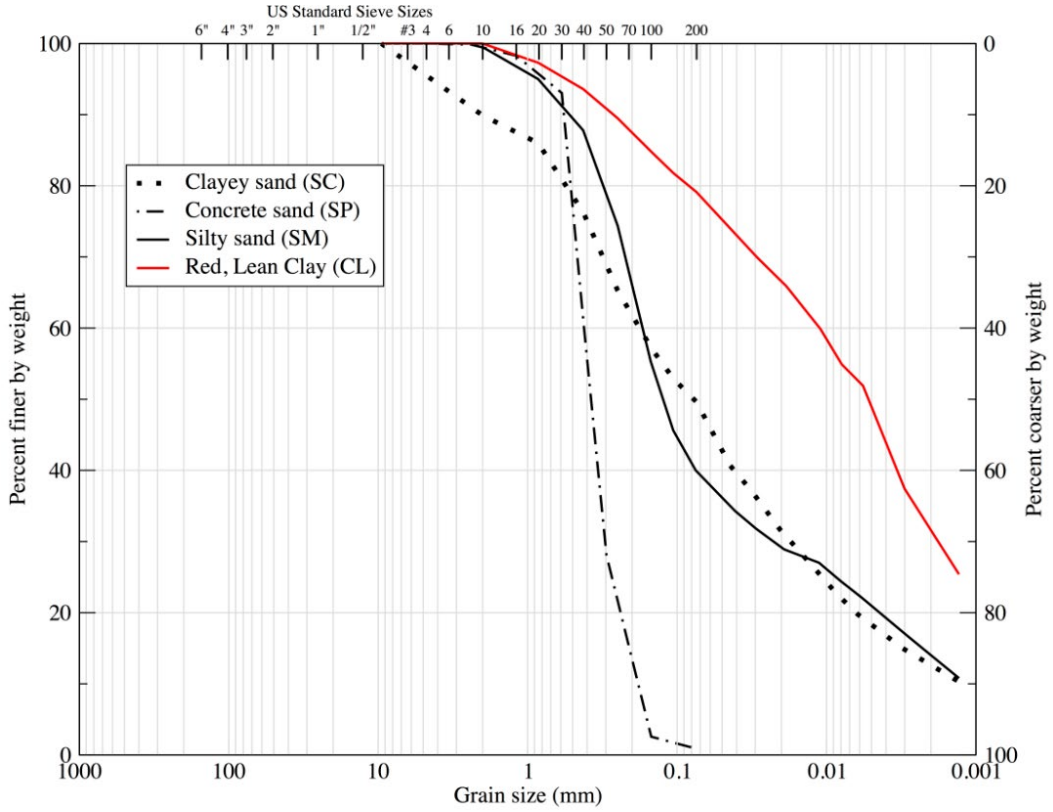

Fig. 2 Particle size distribution for the cohesive soil used in this report (Red Lean Clay) compared with the noncohesive soils from Fox et al.[13]

2. Experimental Procedure

2.1 Soil Mechanical Property Determination Procedures

Particle size distributions were determined by placing the soil on top of a series of progressively finer sieves and observing the proportion of the soil retained on each of the sieves. A hydrometer test was used to determine distributions of particles less than a nominal size of 0.075 mm in accordance with ASTM D-422[16] and D-2487.[17] Experimental determination of the quasi-static properties of the clay was performed at the US Army Engineer Research and Development Center in Vicksburg, Mississippi. These properties were determined by means of experiments that involved uniaxial strain-stress-path pressure–volume relations and triaxial compression failure relations. A more detailed description of the soil characterization experiments is given in Fox et al.[13]

2.2 Small-Scale Buried Blast Procedures

The soil was first sieved using a 4.75-mm (No. 4) sieve and then oven-dried for 24 h in accordance with ASTM D2216.[18] The amount of water mass required to reach the target water content was then added to the dried soil by carefully spraying water on the soil with a hand sprayer as it was being mixed in a commercial concrete mixer. The soil was then stored in a watertight container for an additional 12 h to ensure the homogeneity of the mixture.

The soil mixture was then placed into the test container, or soil pot, in lift thicknesses between 0.5 and 1 inch, and then leveled. A 20-ton hydraulic press with a custom cylindrical metal ram was used to apply the required amount of compaction effort. After each lift was compacted, the top surface was roughened to assist bonding between the layer already in place and the new layer being added. This process was repeated until the soil pot was completely filled. Through this process, a relationship was developed involving the compaction effort, air-volume fraction, and water content, as discussed in Section 4.2.

The experimental setup is scaled from conditions for a full-sized tactical vehicle subjected to a buried blast event. In the representative event, the standoff distance, measured from soil surface to the bottom of vehicles, is 406.4 mm; the depth of burial, measured from top of charge to soil surface, is 101.6 mm; and the threat charge mass is 4.54 kg of TNT.

Application of Hopkinson's scaling laws to the representative setup using a charge mass of 4.4 g results in a scale factor of 10.1. As the scaled charge is well below the critical diameter of TNT, the explosive charges used Detasheet C (63% PETN and 37% plasticizer) and RP-501 detonators. Each detonator contained 169 mg of PETN and 227 mg of HMX explosive. The total mass of each Detasheet C charge was 6.36 g so that the net mass of PETN contributed by the Detasheet C, 4.00 g, brought the total amount of explosive in each of the charges to 4.4 g. The charges had an aspect ratio of approximately 1.69:1, diameter to height, and were right circular cylinders. The charge was buried in the center of the soil pot at a depth of burial of 10 mm to the top of the charge with a 40-mm standoff distance from the surface of the soil to the bottom of the target. The container size was computationally verified to be large enough to rule out any boundary effect both from side walls and the bottom of the soil pot. In other words, our container was large enough to prevent stress waves from the bottom and sides affecting our results.

The target was simplified to a flat, cylindrical plate that weighed 10.5 kg and was fabricated from 50-mm-thick 6061-T6 aluminum plate with a diameter of

304.8 mm, the same diameter as the soil container. This plate diameter was computationally verified to be sufficient to capture all of the ejected material from the explosive detonation. A drawing of the charge and experimental setup is shown in Fig. 3.

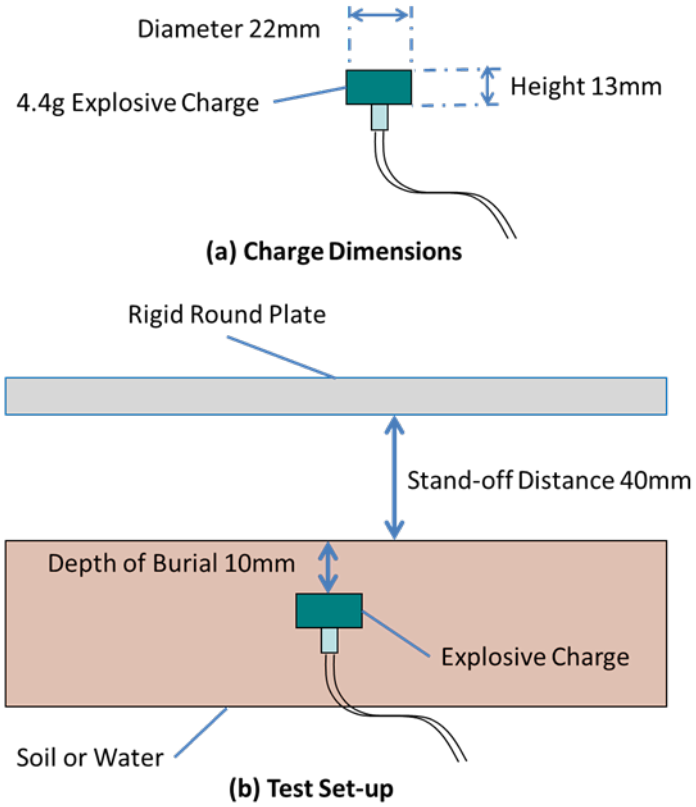

Fig. 3 Diagram of experimental setup (not to scale)

Four fiducial markers on the top of the target plate were used to optically track the plate displacement with a Phantom 12.1 high-speed video camera operating at a framing rate of about 21,000 frames per second. The slope of the plate displacement versus time curve over the first inch of travel was used to determine the initial velocity of the plate. This velocity was multiplied by the mass of the target plate to determine impulse. Figure 4a shows the filled soil pot with the charge emplaced before the charge is covered with soil. Figure 4b shows the experimental setup prior to detonation.

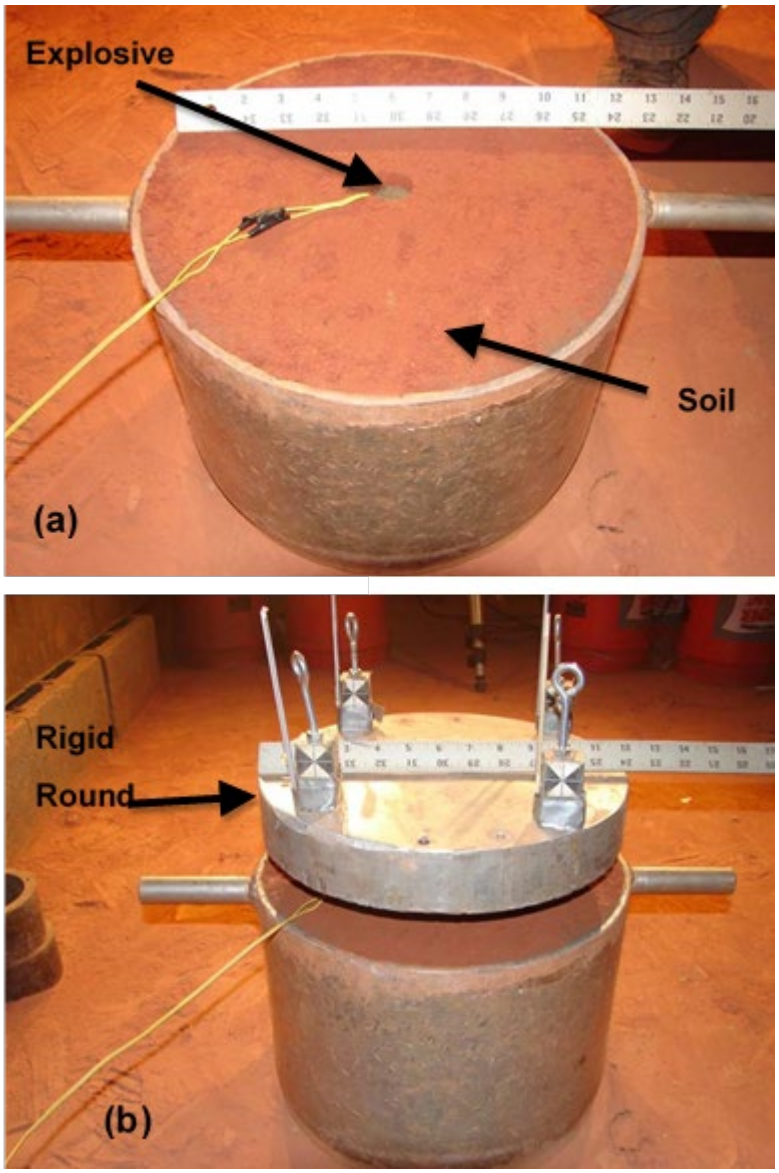

Fig. 4 Experimental setup: (a) filled soil pot with emplaced charge and (b) full setup

2.3 Small-Scale Air-Blast Experimental Procedures

In addition to the buried charge tests, three air-blast tests were conducted to provide a reference for the buried charge tests. In the air-blast tests, the same target plate used in the buried charge tests was suspended sufficiently far above the floor of the test facility so reflected shock waves would not impart additional momentum to the target. As shown in Fig. 5, the charge was mounted on a thin metal shaft that was held in place by a mass on the floor. The top face of the charge was positioned at a distance of 50 mm from the bottom face of the target to match the standoff distance plus depth of burial from the buried tests.

Fig. 5 Air-blast test setup

3. Experimental Results

3.1 High-Pressure Soil Quasi-Static Characterization

Figures 6–8 show the volumetric and yield behavior based on direct physical testing of remolded samples of the clay at four initial emplacement conditions. Three of the emplacement conditions were for partially saturated clay; the fourth for an air-volume fraction of 0.37 and $w = 0$ represented the behavior of dry clay. In Fig. 6, the volumetric stress–strain behavior of the clay is shown with positive strain in compression. As is typical for porous soils, it can be seen that the bulk modulus of the clay is bimodal for the partial saturated emplacements, with the pressure in the clay moderately increasing with increasing compression until the point at which the voids disappear and the soil reaches a saturated state. Beyond the saturated state, the modulus increases significantly as evidenced by the much higher rate of increasing pressure with increasing compression.

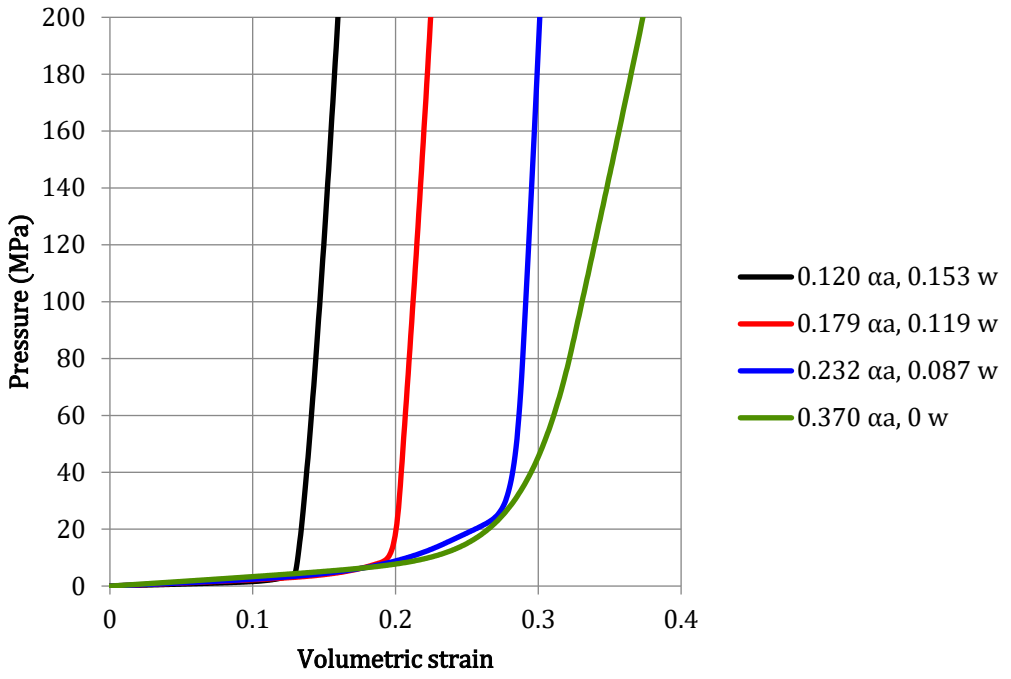

Fig. 6 Stress–strain behavior of clay at four emplacement conditions

Figure 7 shows the pressure-dependent yield surface of the soil for the four initial emplacement conditions. It has been observed that the pressure-dependent yield behavior of the clay follows the exponential relation

$$\boldsymbol{\sigma_y = k_1 - k_2 \exp(k_3 p)}, \tag{1}$$

where σ_y is the yield strength, p is the pressure, and k_1, k_2, and k_3 are constants. With this type of description of the yield behavior, the yield surfaces for the various soil emplacements overlay one another at lower pressure levels. Then, with increasing pressure, the volume of the air component of the soil becomes very small and the soil approaches an asymptotic level of yield strength.

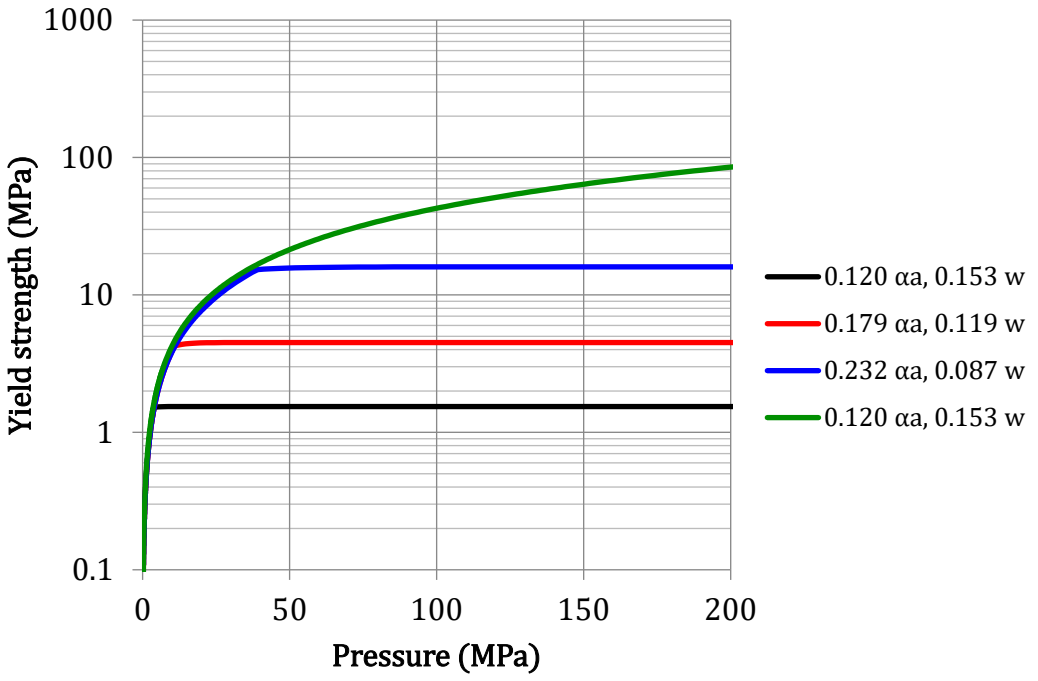

Fig. 7 Pressure-dependent yield strength of clay at four different emplacement conditions

Figure 8 shows the parametric relation between the water content w and the asymptotic yield strength $\sigma_{y,a}$ for each of the four initial soil conditions. $\sigma_{y,a}$ exhibits an exponential dependence on w according to the relation

$$\boldsymbol{\sigma_{y,a} = k_4 \exp(k_5 w)}, \tag{2}$$

where k_4 and k_5 are constants associated with the soil and, for the solid line shown in Fig. 8, were determined by means of a least-squares fit. $\sigma_{y,a}$ decreases with increasing water content because an increase in water content—the ratio of the mass of water to the mass of soil solids in a control volume of the soil—resulted in a reduction of the friction between the solid soil particles. This was a result of the tendency of increasing water content to reduce the inter-particle contact forces after the soil has been compressed beyond the point of saturation.

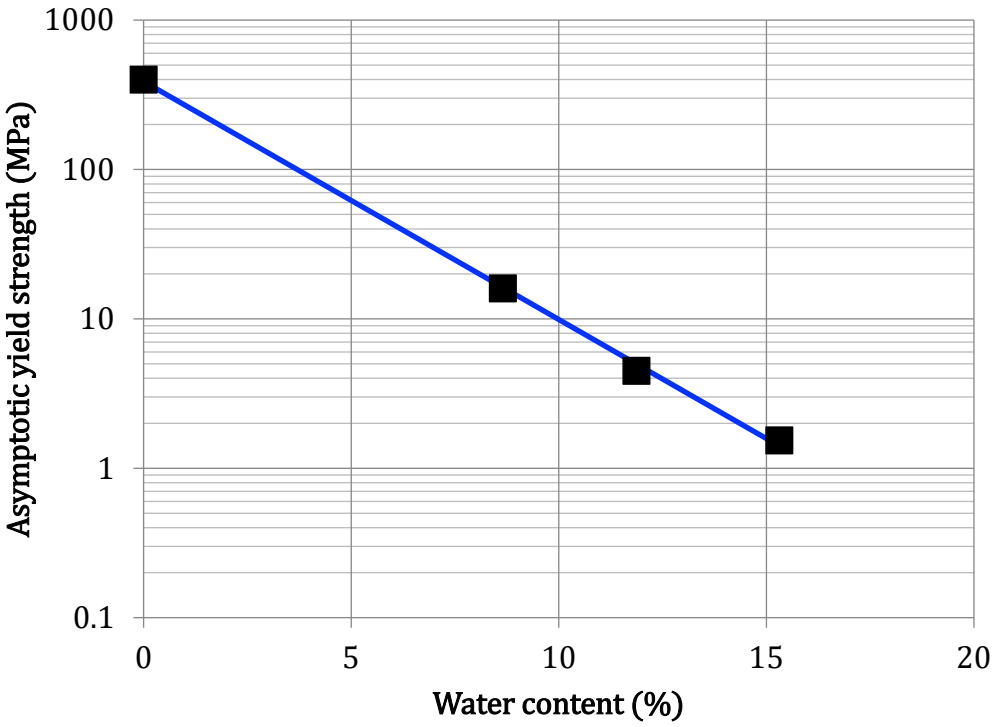

Fig. 8 Asymptotic values of clay yield strength as a function of water content for four emplacement conditions

3.2 Air-Blast Results

Air-blast results are summarized in Table 1.

Table 1 Air-blast results

Test no.	Impulse (*N.s*)
50	6.678
51	6.110
52	6.512
Mean	6.433
STD	0.238

3.3 Small-Scale Buried Charge Results

Experimental results are summarized in Table A-1 in the Appendix. Figure 9 is a stacked bar plot showing the volumetric proportions of air, water, and soil solids for each experiment. The experiments are sorted in descending air-void fraction.

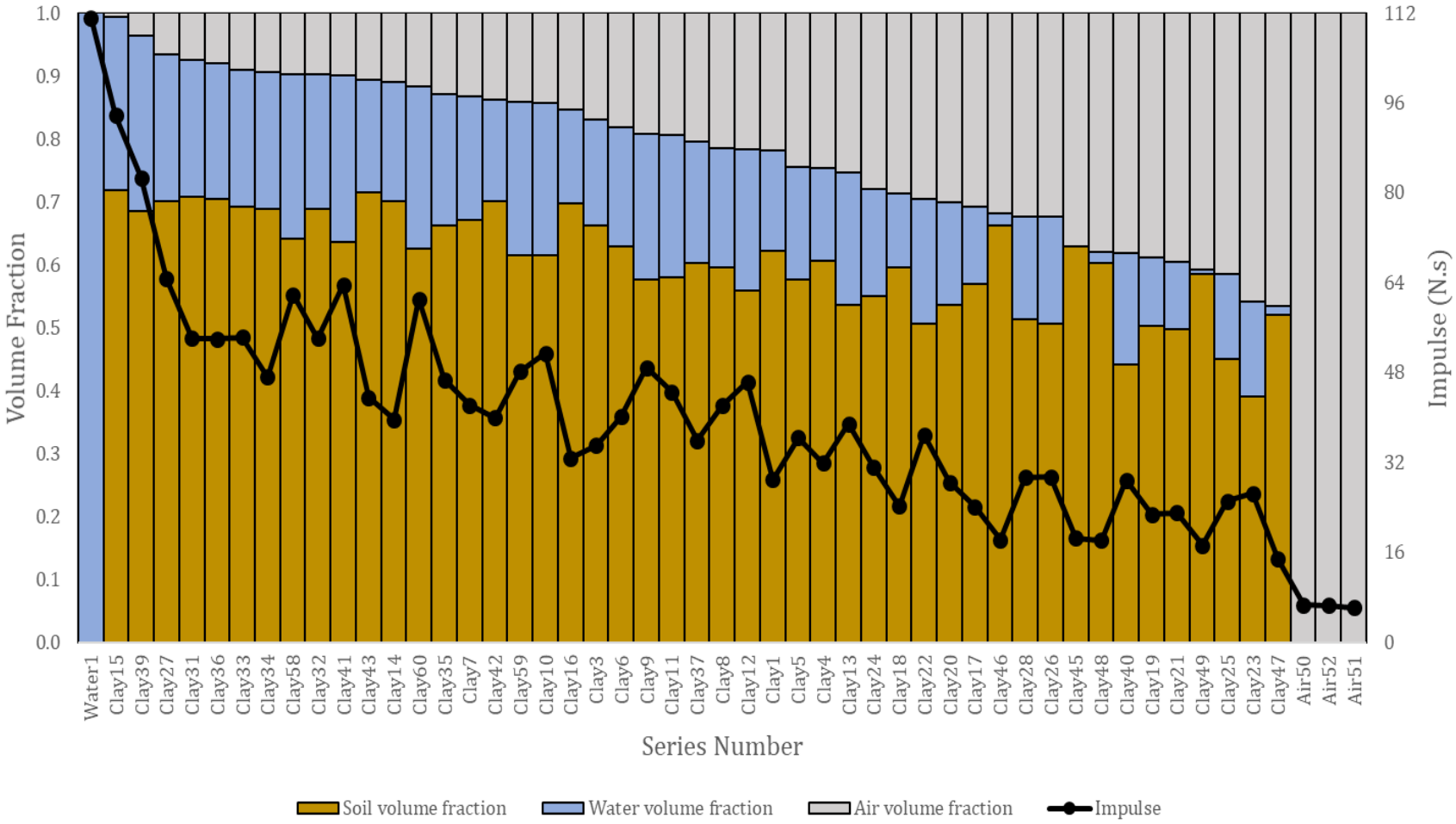

Fig. 9 Stacked bar plots of volume content and impulse. Experiments sorted in descending air-volume fraction.

A total of 50 buried blast experiments were conducted, of which three results were discarded due to the target plate showing too much rotation in its initial displacement, suggesting that the charge was located slightly off the center point of the plate.

The 47 valid buried blast experiments are organized into four experimental series named for their target water content value (Table 2).

Table 2 Experimental series

Series name	Target (w)	Mean (w)	Standard deviation	Min value (w)	Max value (w)
w = 8.65%	0.0865	0.0874	0.0744	0.0744	0.1016
w = 11.87%	0.1187	0.1170	0.0041	0.1101	0.1266
w = 15.31%	0.1531	0.1493	0.0035	0.1426	0.1555
w = 0%	0	0.0072	0.0041	0.0002	0.0108

4. Discussion

4.1 Predetonative Soil State

The three-phase soil model is a geotechnical abstraction of a soil system in which a volume of soil consists of solid particles (forming a soil skeleton) with void spaces between particles. This void space can be filled with any combination of water and/or air such that the volumetric representation of the mixture can be expressed as $a_s + a_w + a_a = 1$, where a_s, a_w, and a_a represent the volume fractions of soil, air, and water, respectively. Ideally, the dynamic response of a soil system would depend on the volume fractions of the three primary phases, but interactions between the soil and water and the water and air phases can influence the high-rate mechanical response of soils while being difficult to quantify.

Physicochemical properties of clay minerals along with pore volume and pore morphology results in complex interactions between a clay-containing solid phase and the water phase. The surface of clay mineral particles has a net negative charge to which the positive ions and polar water molecules will align and bond, forming a double layer near the surface of a clay particle. Water content in clay-containing soils can be divided into two categories: adsorbed water content and a free water content, with the adsorbed water content being either strongly or weakly bonded. Adsorbed water will not have the same constitutive properties (i.e., density and compressibility) as free water content.

If the air phase is continuous, the air–water interface (contractile skin) results in surface tension in the soil skeleton that would not occur if the water phase was

continuous. Additionally, when the air phase consists of occluded air bubbles, the miscible mixture of air and water is more compressible than an immiscible mixture would be.

For this report the parameters used to control the predetonative soil state were the amount of compaction effort applied and water content.

Figure 10 shows the compaction effort required to achieve a given air-volume fraction for each of the four water content series. In general, the amount of compaction effort required to reach a given air-volume fraction increases as water content decreases.

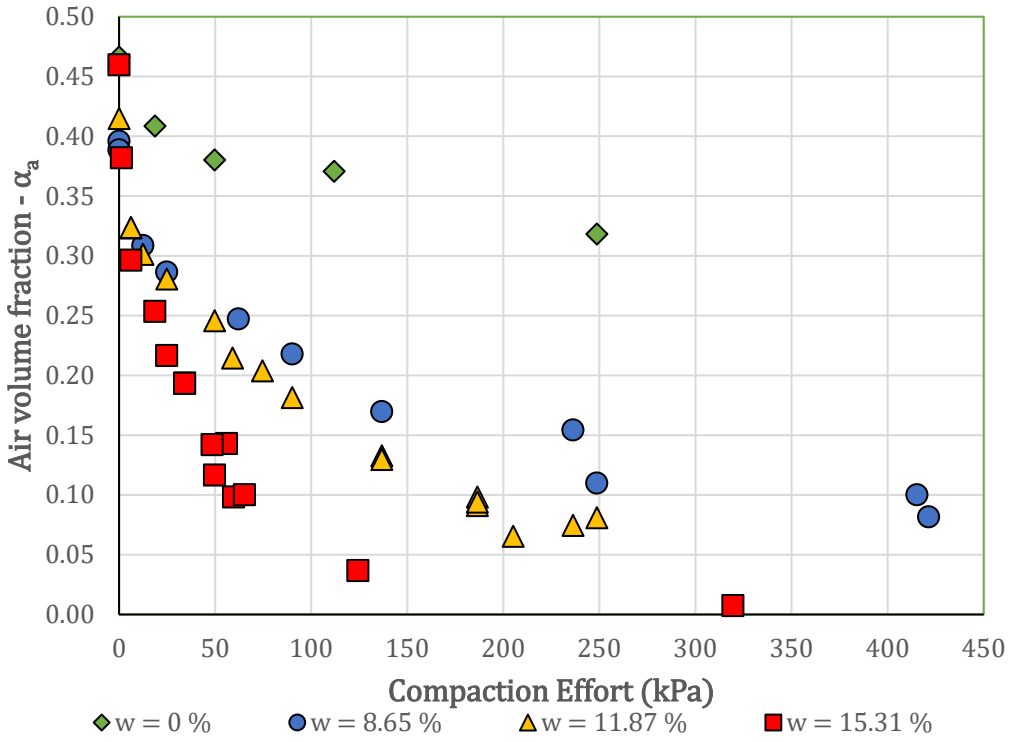

Fig. 10 Compaction effort required to reach a given air-void fraction for the four water-content series used in this report

A 20-ton press at the Dynamics Effects Laboratory at the University of Maryland, College Park, was used for all but two test conditions. Achieving an air-volume content less than 10% in the w = 8.65% series required a compaction effort greater than 350 kPa, so those samples were prepared using a 40-ton press located at the US Army Combat Capabilities Development Command Army Research Laboratory's Small Scale Buried Blast Facility on Aberdeen Proving Ground, Maryland.

In an effort to determine the boundaries of allowable soil states that the soil under consideration can exist in a three-phase soil model assumption, both the standard Proctor (StdP) compaction test (ASTM D698 Method A17[19]) and the modified Proctor (ModP) compaction test (ASTM D1557[20]) were conducted. The Atterberg limits were determined in accordance with ASTM D4318–17e1.[21]

Proctor tests establish an optimum dry density and water content value for given compaction efforts. Proctor compaction test procedures typically do not require conditions that span the entire water content and dry density space possible for the compaction effort used. To obtain complete compaction curves, therefore Eq. 6 from Li and Sego[22] was used to fit the StdP laboratory test values and then the resulting parameters were used to derive iso-compaction curves for the remaining experimental data.

Where the experimental data indicated a so-called double-peaked compaction curve, as occurred at soil states below approximately $a_s = 0.64$, methods from Al-Badran and Schanz[23] were used. This process not only establishes a complete compaction curve for a given compaction effort but also determines the relationship between the static compaction effort used in this report and the more dynamic compaction used in the ASTM Proctor procedures.

In Fig. 11, the maximum compaction effort, the iso-compaction line is approximated by using the model parameters from the fit to the StdP data with the average of minimum void ratio values for CL soil types from Hough[24] and then assuming that this minimum void ratio value was for soil in the dry condition. It is then assumed that compaction efforts greater than the maximum value would result in fractured soil particulates.

As described previously, the minimum compaction effort iso-compaction line was established by using methods from Al-Badran and Schanz[23] fitted to experimental data in which soil beds were constructed with no compaction effort. This minimum compaction effort line is assumed to pass through the lowest dry density a saturated soil can achieve.

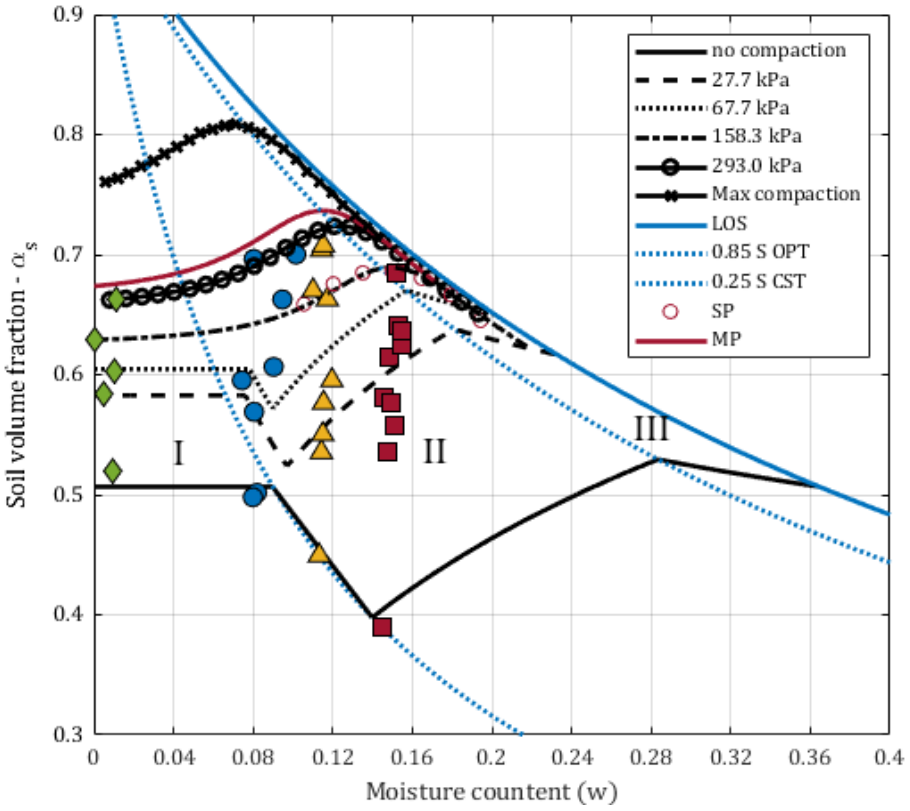

Fig. 11 Lines of iso-compaction effort in Proctor space. SP is the standard Proctor test, and MP is the modified Proctor test. LOS is line of saturation, 0.85 S OPT is the saturation at optimal moisture and density; assumed constant. 0.25 S CST is the saturation at the compaction sensitivity threshold; also assumed constant. Experimental data points shown are only those used to fit their respective iso-compaction effort.

For the analysis in this report, the minimum and maximum iso-compaction lines, defined by the no-compaction-effort emplacement condition and an extrapolation from the soils minimum void ratio, respectively, together with the line of saturation (LOS)-bound allowable soil states.

From Fig. 11, four lines of constant saturation are used to define three regions of interest: 1) the LOS, identical to the zero air-volume fraction line, which is a function of the soil's specific gravity alone; 2) the line compaction sensitivity threshold (CST), whose constant saturation value of 0.25 is taken from methods in Al-Badran et al.[21] fitted to the no-compaction effort experimental data; 3) the line of optimum moisture and density (OPT); and 4) the zero-saturation line.

In Region I, between the zero-moisture content line and the CST line, under a constant compaction effort, dry density remains relatively constant with the addition of water content. This phenomenology is attributed to the moisture content being insufficient to provide "lubrication" for soil consolidation. Moisture content in this region will be largely in the adsorbed category; the air phase will be

continuous; and the water phase will be discontinuous. For soil states less than approximately $0.64\ a_s$ that are on or near the CST line, surface tension forces in the air–water interface causes soil hardening (see Al-Badran and Schanz[23]) resulting in a decrease in soil-volume fraction with an increase in moisture content; that is, the soil maintains a constant level of saturation until the minimum density level is reached for that compaction effort, which results in the double peaked iso-compaction lines seen in Fig. 11. This behavior indicates a dependency on pore type (classification of statistical pore volume: macropore, micropore, etc.).

In Region II, between the CST line and the OPT line, density increases with the addition of moisture content until a maximum (optimum) dry density is reached at an optimum moisture content. Moisture content transitions from being predominately adsorbed to the mixture of adsorbed and free water content allowed by pore type at optimum dry density. The air phase transitions from being continuous to discontinuous while the water phase transitions from discontinuous to continuous.

Region III is from the OPT line to the LOS. Generally, dry density decreases with an increase in moisture content in this region as the addition of water displaces soil solids. Li and Sego[22] and Al-Badran and Schanz[23] make different assumptions about the behavior in this region: Li and Sego assume a maximal saturation value less than one that is approximated as a constant for all compaction efforts, whereas Al-Badran and Schanz allow for saturated soils. Any air-volume content in this region is discontinuous and has a higher probability of being in a miscible mixture with the water phase.

Figure 12 shows the bounds of allowable soil states as well as the three regions of interest in air-volume fraction and water content space. In Fox et al.,[13] a relationship between air-volume fraction and impulse delivered was demonstrated. The analysis in this section establishes the range of air-volume fractions that a given soil can achieve for a given moisture content. For example, in Fig. 12, tracing the 0.04 moisture content line between the minimum and maximum compaction efforts spans the allowable air-volume fraction that the soil can achieve and therefore constrains the range of impulsive responses for that moisture content.

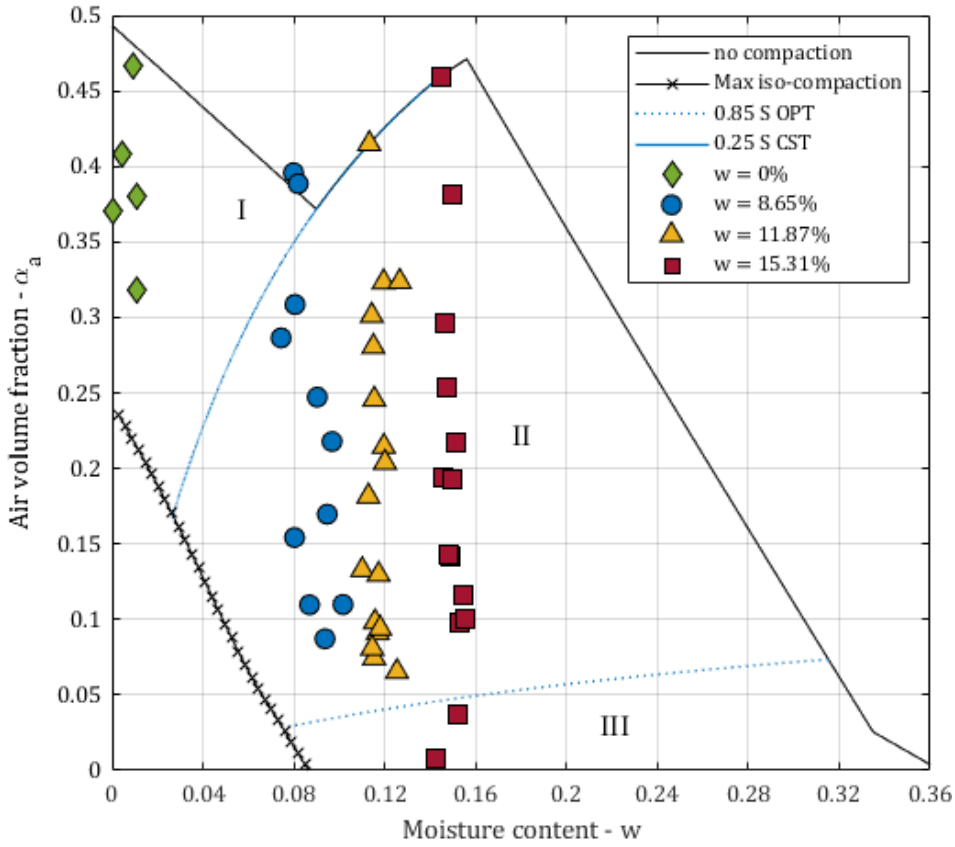

Fig. 12 Allowable soil states and the regions of interest in air-volume fraction and water content space

4.2 Impulsive Response as a Function of Three-Phase Soil Model Parameters

In Figs. 13a through 13c, impulsive response versus the volumetric parameters from the three-phase soil model are plotted.

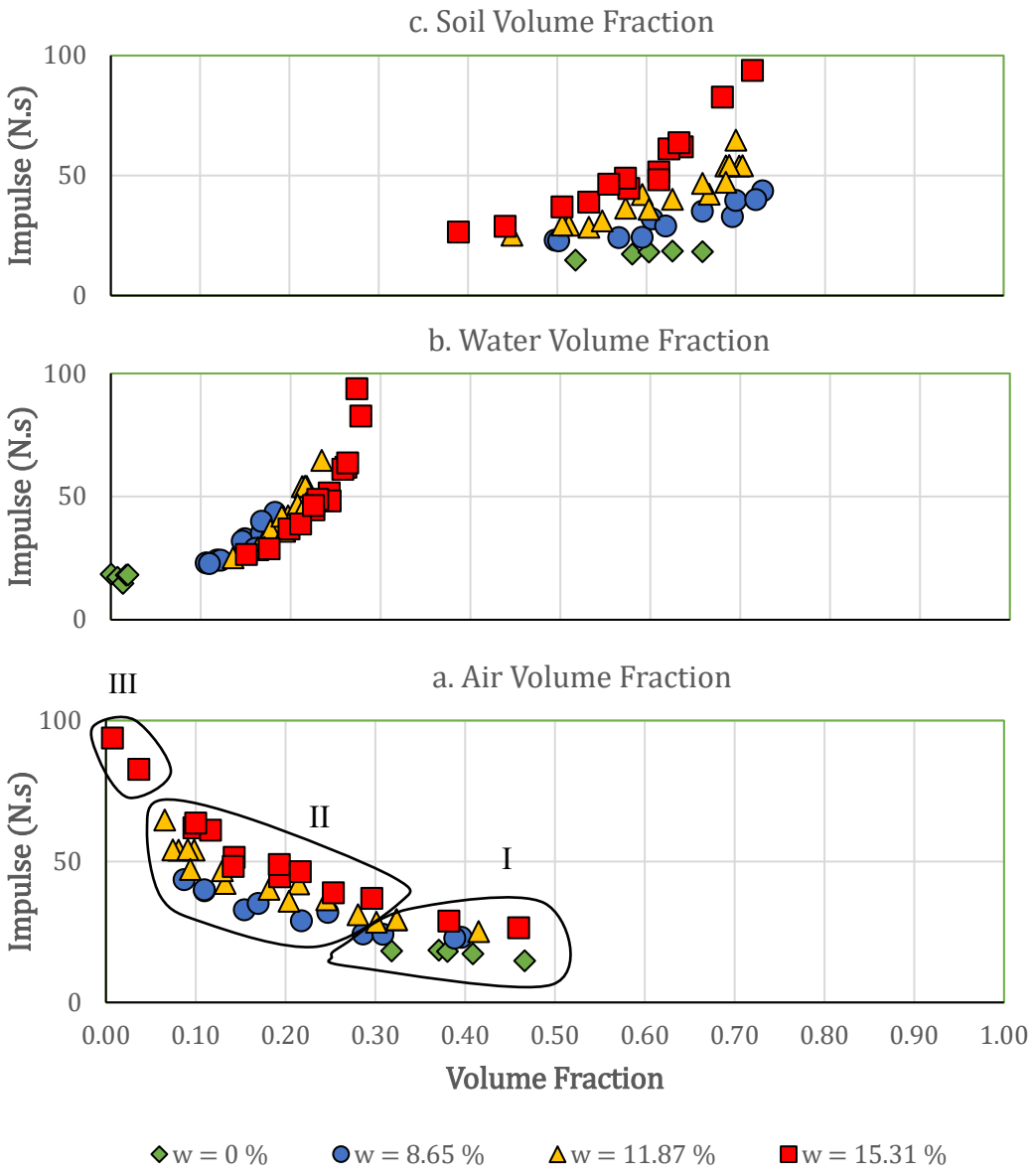

Fig. 13 Impulsive response vs. three-phase soil model parameters: a) air-volume fraction, b) water-volume fraction, and c) soil-volume fraction. Roman numerals I, II, and III in 13a correspond to the three regions of interest from Section 4.1.

Figure 13a is impulsive response versus air-volume fraction (α_a) delineated by the four water-content series from this report and the soil-state region of interest. Taken as a whole, the trend is similar to the impulse versus air-volume fraction response from the soils tested in Fox et al.[13] (Fig. 1) but clearly highlights, at least for the clay soil used in this work, a dependence on moisture content and the predetonative soil state region. Generally:

- Impulsive response is inversely proportional to air-volume fraction as would be expected from the volumetric stress–strain relationship shown in Fig. 6.
- There is an additional dependence on water content. Impulse appears to have an inverse relationship to asymptotic yield stress as from Fig. 8 (i.e., an increase in moisture content results in a decrease in yield stress).
- Sensitivity to water content decreases as air-volume fraction increases. Some of this can be explained by the fact that dryer soils can only exist at a relatively narrow range of air-volume fractions compared with wetter soils.
- For the same air-volume fraction, soils with larger water-volume fractions produce more impulse; this is particularly apparent in the stacked plots of Fig. 10. This is identical to the statement that a low-density soils with high moisture content can produce more impulse than a dense soil with low moisture content.
- Soils in Region I have a low sensitivity to a decrease in air-volume fraction.
- Soils in Regions II and III are progressively more sensitive to decreases in air-volume fraction.

If you disregard the slurried state, it is the author's experience that, all other factors being equal, the largest practical impulse is achieved when the water-volume fraction is 1; that is, in water, hereafter referred to as the hydrodynamic response. Based on results from Fox et al.[13] and a validating experiment in similar experimental conditions (target to charge distance, target surface area, and soil pot dimension) as was used for the buried experiments in this report, a mean hydrodynamic response, $I_w = 111.08\ N.s.$, is established.

If we assume that the hydrodynamic response is the maximal impulsive response, then an analysis of the data in Fig. 13b indicates there is a water-volume fraction less than 1, above which all impulsive responses will be the hydrodynamic response (I_w).

As determined by ASTM D4318–17el,[21] the liquid limit (LL) for the soil is 0.21, and the plastic limit (PL) is 0.10. Water-volume fraction for a saturated soil as a function of water content is $\alpha_{w\,saturation} = 1 - \frac{1}{1+wG_s}$, which results in a water-volume fraction of 0.21 for the PL and 0.36 for the LL for the saturated soil. For reference, the maximum water-volume fraction achievable under the analysis in Section 5.2 (see Fig. 11) is 0.49.

This would indicate that the functional form of impulse response versus water-volume content is a sigmoid curve. A generalized logistic model fit to the impulse versus water-volume fraction data shown in Fig. 13b: The upper asymptote set to the hydrodynamic value results in lower inflection points close to what the water-volume fraction would be at the CST line—$S = 0.25$ or in this case $\alpha_w = 0.10$—depending on soil-volume fraction chosen, and the upper inflection point being the water-volume fraction for a saturated soil at the liquid limit. In general:

- In soils that demonstrate a compaction sensitivity threshold, impulsive response will be insensitive to water-volume fractions below the CST line.
- There is an upper water-volume fraction value above which all impulsive responses will be the hydrodynamic response, regardless of dry density. This upper water-volume fraction value has some a correlation to the water-volume content for a saturated soil at the liquid limit.
- Soils states above the upper water-volume fraction value can be unsaturated (have nonzero air-volume fractions) and still produce the hydrodynamic result.
- There is a dry density above which a soil will always produce less than the hydrodynamic response, regardless of level of saturation.

The multimodal response of impulse versus air-volume fraction indicates that all pore volumes are not equivalent when it comes to impulsive response. The clay containing solid phase's interaction with the water phase is both physicochemical and morphological. According to Chao and Ning,[25] pore water density in clay soils can range from 1.6 to 0.9 $\frac{g}{cm^3}$, depending on the spatial distance from the pore boundary the density is measured. Dense clay-containing soils with relatively small pore volumes will have a higher mean water density than the same pore volume containing free water content. Therefore, by Table A-1 in the Appendix, these soils have a higher air-volume fraction leading to a lower impulsive response. This implies that there are soil densities of fine-grained and clay-containing soils above which the mean pore volume will be insufficient to support a continuous free-water phase and therefore result in the hydrodynamic response. Conversely, there are soil densities whose moisture content at saturation will be too low to result in an asymptotic yield strength low enough to provide the hydrodynamic response.

4.3 Impulsive Response as a Function of Coupling Parameters

Here, a coupling parameter is a soil parameter that is a ratio of other soil parameters. Figure 14 shows impulse versus gravimetric water content, generally, for a constant solid-volume fraction there is an increase in impulsive response with an increase in

water content, while the rate of impulsive response as a function of moisture content is dependent on porosity. Air-volume fraction can be reformulated as $\alpha_a = 1 - \alpha_s(1 + wG_s)$, where an increase in solid-volume fraction or water content will decrease air-volume fraction and correspondingly result in a higher impulsive response (Fig. 14). For this reason air-volume fraction is a better first-order predictor of impulsive response than is water content alone.

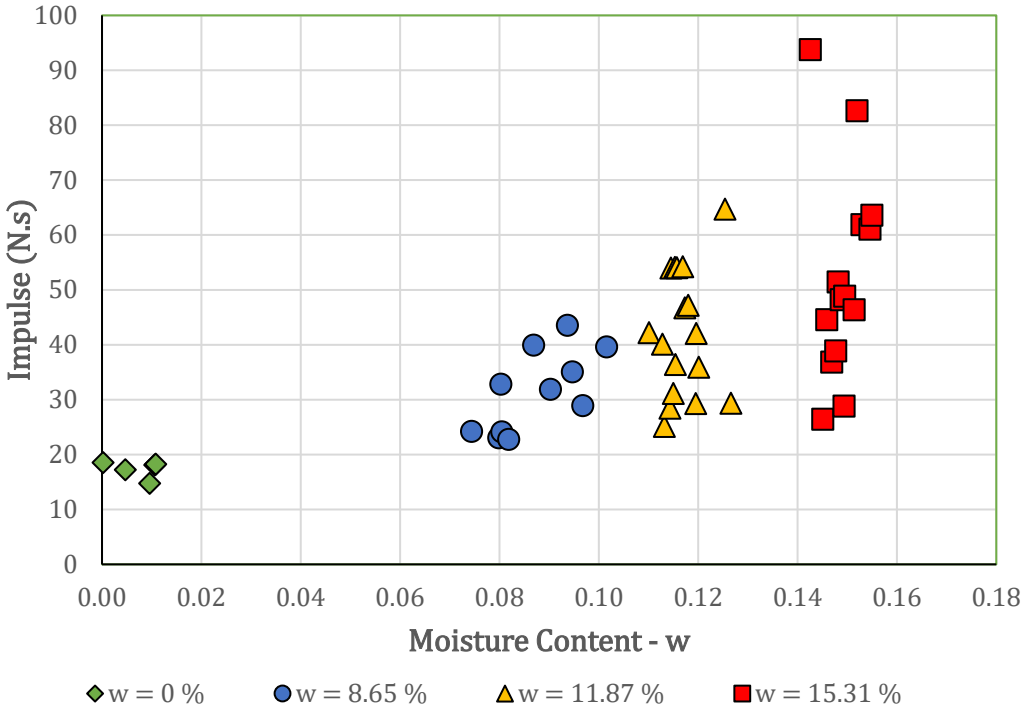

Fig. 14 Impulse vs. gravimetric water content

Conceptually, saturation is an ideal coupling parameter. If you start with a dry soil, for which air-volume fraction and porosity are equivalent, an increase in saturation represents the fraction of that porosity that is filled with water. From Fig.15 we can see that there is a good correlation between impulsive response and saturation, with nearly linear impulsive response in each soil state region.

What is missing for both saturation and water-volume fraction is the effect of porosity (pore type) and the effects soil solids and water interactions will have on the impulse that a given saturation level produces. Saturated high-porosity soils result in more impulse than saturated low-porosity soils. The impulsive response of both high and low porosity soils appears to be insensitive to low levels of saturation.

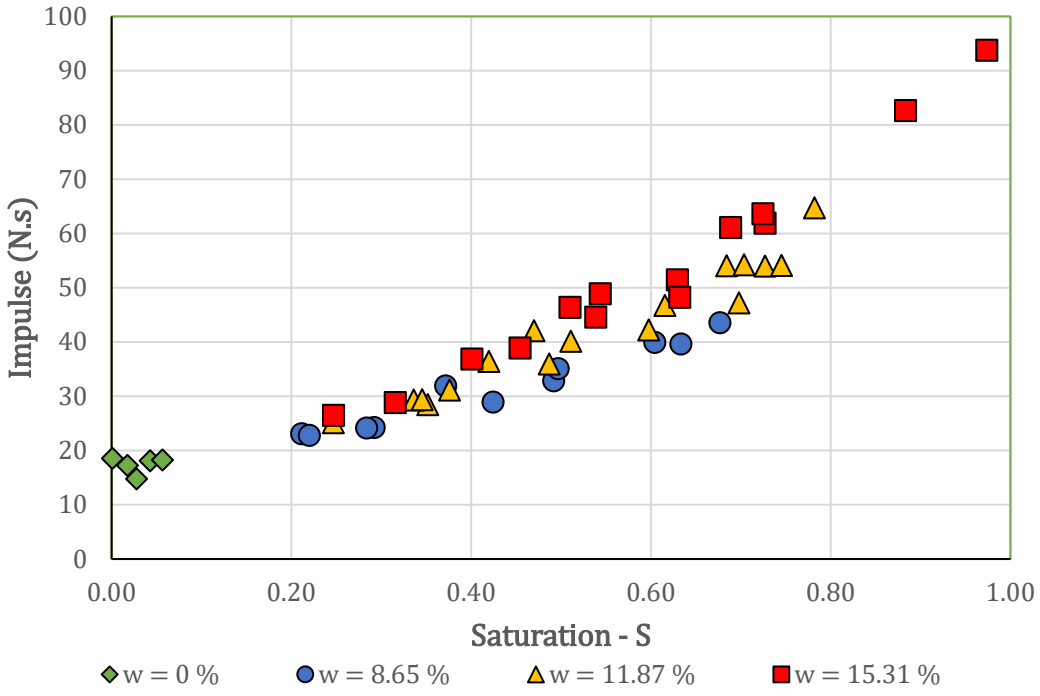

Fig. 15 Impulsive vs. saturation

In an attempt to qualify the impulsive response as a function of both porosity and saturation, a Weibull growth model in the form of Eq. 3 was fit to the data using an iterative process that minimized the sum of squared errors (SSE) of the dataset as a whole but also attempted to minimize the difference in magnitude of the SSE between moisture content series.

$$\boldsymbol{I_b(\alpha_s, \alpha_w, S) = I_w - (I_w - I_{dry})e^{-(b\alpha_w)^{\delta}}} \quad (3)$$

with the dry-soil impulse I_{dry}

$$I_{dry} = I_a \cdot e^{x1 \cdot \alpha_s}$$

growth rate b a function of saturation

$$b = x2^S$$

and δ, a shape parameter, also a function of saturation

$$\delta = x3^S$$

resulting in an adjusted coefficient of determination of 0.983 with coefficients, $x1$ = 1.4832, $x2$ = 4.7489, and $x3$ = 2.2988. The results are plotted in Fig. 16.

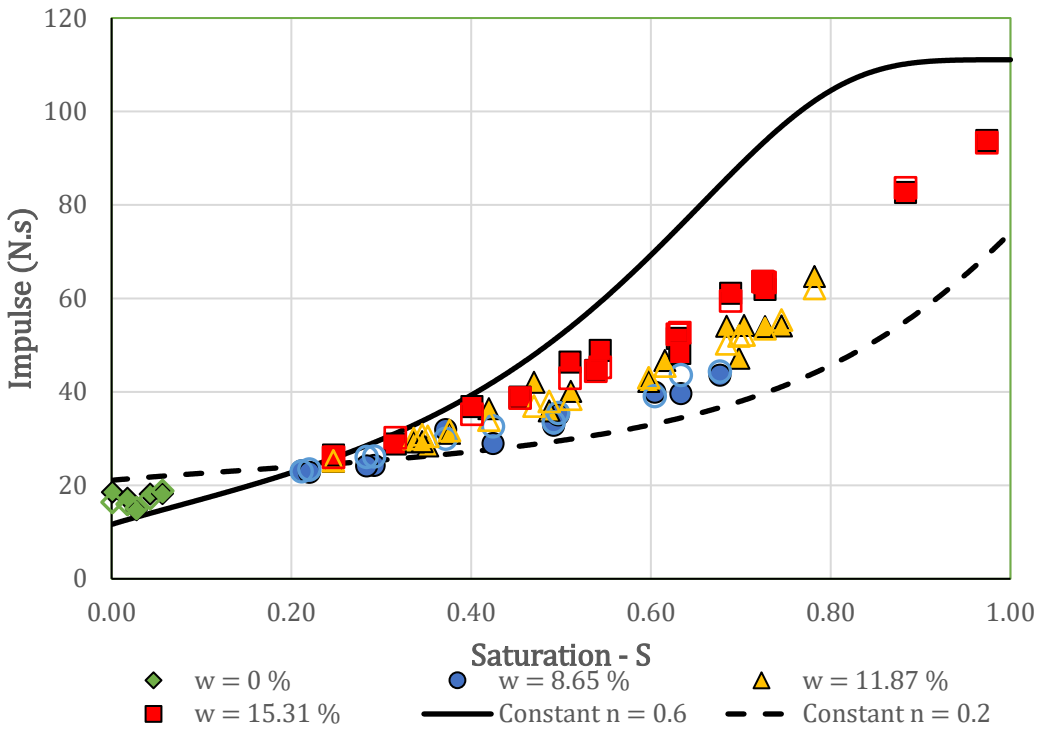

Fig. 16 Impulse vs. saturation results from Eq. 7. Solid markers are experimental data and hollow markers are model results. Solid line is impulsive response for a constant porosity of 0.6 and dashed line is for a constant porosity of 0.2 by Eq. 7.

Also plotted in Fig. 16 are impulsive responses for a constant porosity of 0.2 and 0.6 by Eq. 3. In Region I, below a saturation level of approximately 0.25 (the constant CST saturation value identified in Section 4.1), impulsive response is dominated by soil density. At the CST saturation value, impulsive response is nearly a constant for all soil densities. After the CST saturation value, the high-porosity response curve increases rapidly, passing through the LL at a saturation of 0.37 and reaching the hydrodynamic response at a saturation of approximately 0.85 with a moisture content of 0.48, an approximately 9.5-fold increase in impulse over the dry soil response. The low-porosity curve doubles the dry soil impulsive response at a saturation value of approximately 0.75 and is only approximately 3.9 times the dry-soil impulsive response when saturated at a moisture content of 0.094, just under the PL.

Using the empirical model given in Eq. 3 and the bounds of allowable soil states from Section 4.1, impulsive response as a function of both air-volume fraction and moisture content is plotted in Fig. 17.

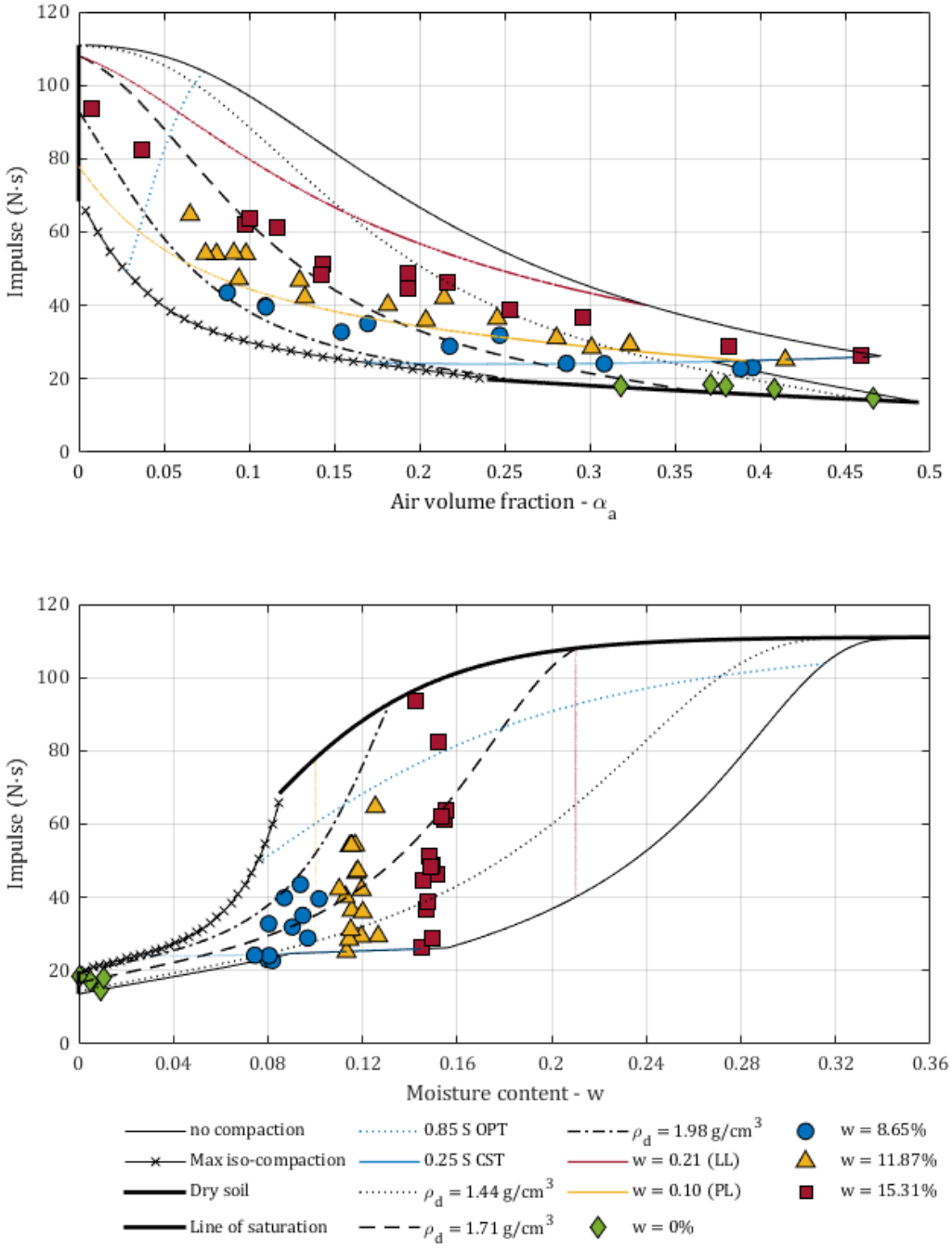

Fig. 17 Impulse vs. air-volume fraction and moisture content according to Eq. 3. Minimum and maximum iso-compaction defines the bounds of allowable air-volume fraction values. Dashed lines are lines of constant dry density; colored lines are lines of constant moisture content.

5. Summary and Conclusion

We conducted a series of 47 buried blast tests using a lean clay soil, 25% of the particles of which are less than 0.001 mm (plus three air-blast tests and one water test). We used 4.4-g explosive charges to represent a full size 4.54-kg charge buried 101.6 mm deep to the top of the charge. The bottom of the representative vehicle target would have a standoff distance of 408.4 mm.

We examined how predetonative soil state properties derived from the three-phase soil model assumption affect impulse delivered. In Fox et al.,[13] it was found that air-volume fraction correlated well with the impulse delivered for the noncohesive soils evaluated.

For the cohesive, lean clay soil used for this series of experiments, we found that the single three-phase soil model parameter that is the best first-order predictor for impulse delivered was also air-volume fraction with these caveats:

- Impulsive response is inversely proportional to air-volume fraction.
- There is an additional dependence on water content.
- Sensitivity to water content decreases as air-volume fraction increases.
- For the same air-volume fraction, soils with larger water-volume fractions produce more impulse.
- The sensitivity of impulsive response to a decrease in air-volume fraction is dependent on the physicochemical and morphological interaction between clay minerals and the water content, whether the water phase is continuous and if the pore volume is sufficiently large to support free water content.

Additionally, for the cohesive soil examined in this report, the model identified that there are possible correlations between the Atterberg limits and impulse delivered; the soil-volume content for a saturated soil at the liquid limit appears to be the maximum dry density for which the soil can achieve the hydrodynamic response; dry densities above this value can never achieve the hydrodynamic response; and it is possible for soil below this value to achieve the hydrodynamic response while having nonzero air-volume fraction.

The functional form of impulsive response versus air-volume fraction obtained by the model given in Eq. 3 is shaped by the allowable soil states as defined in Section 4.1. (Fig. 11) and the assumption that the magnitude of impulsive response in soil is bounded by the impulse response in air and the hydrodynamic response.

As an example, the region of allowable soil states is smaller for soils with air volume fractions greater than approximately 0.25 α_a, which limits the span of potential impulse response for soils in those states. Conversely, for soils with air-volume fraction between approximately 0.05 and 0.15 α_a (typical results for soils compacted at the Proctor optimum moisture density), the span of potential impulsive response is larger, as there is a larger region of allowable soil states. This highlights the deficiency of single soil parameter prediction of impulsive response for soil states above approximately 0.25 α_a. The span of allowable moisture contents and the relatively insensitivity of impulse from moisture content in this region means that air-volume fraction alone may be a sufficient predictor of impulsive response. Below the 0.25 α_a threshold, the span of allowable soil states is larger and therefore the span of impulsive response and both air-volume fraction and moisture content must be considered for impulsive response predictions.

More work needs to be done in the region of low soil-volume fraction at high water contents primarily to validate the assumption that the hydrodynamic response is the maximal impulsive response for a given experimental condition. It is not an unreasonable assumption to assume that slurried soils may produce more impulse than the pure hydrodynamic condition due to the added density resulting from the presence of soil particles as compared with the hydrodynamic result.

6. References

1. Kolsky H, Lewis JP, Sampson MT, Shearman AC, Snow CI. Splashes from underwater explosions. Philos Trans R Soc London Ser A. 1949;196:397–402.
2. Perkins B. True crater dimensions in various soils and rock. Ballistics Research Laboratory (US); 1954. Memorandum Report No.: 773.
3. Friedman B. Theory of underwater explosion bubbles. Commun Pure Appl Math. 1950;3:177–199.
4. Lampson CW. Final report on effects of underground explosions. Office of Scientific Research and Development (US); 1946. Report No.: 6645.
5. Nordyke MD. Nuclear craters and preliminary theory of the mechanics of explosive crater formation. J Geophys Res. 1961;66:3439–3459.
6. Jackson JG. Analysis of laboratory test data to derive soil constitutive properties. Army Engineer Waterways Experiment Station (US); 1969. Miscellaneous Paper No.: S-69-16.
7. Westine PS. The impulse imparted to targets by the detonation of land mines. The Shock and Vibration Bulletin, Bulletin 42, Part 4. Naval Research Center (US); 1972.
8. Cole RH. Underwater explosions. Dover; 1965.
9. Malme CI, Carbonell JR, Dyer I. Mechanisms in the generation of air blasts by underwater explosions. Naval Ordnance Laboratory (US); 1966. Report No.: 66-88.
10. Fourney WL, Taylor LC, Robeson D. Underwater cratering and channeling with explosives. FragBlast. 1999;3:165–183.
11. Fox DM, Lee JS. The influence of water, dry sand, and unsaturated sand constitutive behavior on the blast response of a rigid target. Int J Impact Eng. 2014;65:163–173.
12. Fourney WL, Leiste U, Hauch A, Jung D. Distribution of specific impulse on vehicles subjected to improvised explosive devices. Blasting Fragment. 2010;4:117–135.
13. Fox DM, Akers SA, Leiste UH, Fourney WL, Windham JE, Lee JS, Ehrgott JQ, Taylor LC. The effects of air filled voids and water content on the momentum transferred from a shallow buried explosive to a rigid target. Int J Impact Eng. 2014;69:182–193.

14. US Army Corp of Engineers. The unified soil classification system. Army Engineer Waterways Experiment Station (US); 1960. Technical Memorandum No.: 3-357.

15. Fourney WL, Leiste U, Bonenberger R, Goodings D. Explosive impulse on plates. FragBlast. 2005;9(1):1–17.

16. ASTM D-422. Standard test method for particle-size analysis of soils. ASTM International; 2014.

17. ASTM D-2487. Standard practice for classification of soils for engineering purposes (unified soil classification system). ASTM International; 2017 May 10.

18. ASTM D2216. Standard test methods for laboratory determination of water (moisture) content of soil and rock by mass. ASTM International; 2019.

19. ASTM D698 Method A. Standard test methods for laboratory compaction characteristics of soil using standard effort (12,400 ft-lbf/ft^3 [600 kN-m/m^3]). ASTM International; 2021.

20. ASTM D1557. Standard test methods for laboratory compaction characteristics of soil using modified effort (56,000 ft-lbf/ft^3 [2,700 kN-m/m^3]). ASTM International; 2021.

21. ASTM D4318–17el. Standard test methods for liquid limit, plastic limit, and plasticity index of soils. ASTM International; 2017.

22. Li H, Sego D. Equation for complete compaction curve of fine-grained soils and its applications. Constructing and controlling compaction of earth fills. In: Shanklin D, Talbot J, Rademacher K, editors. ASTM International, 2000. p. 113–125.

23. Al-Badran Y, Schanz T. Modelling the compaction curve of fine-grained soils. Soils Found. 2014;54(3):426–438.

24. Hough BK. Basic soils engineering. Ronald Press; 1969.

25. Chao Z, Ning L. What is the range of soil water density? Critical reviews with a unified model. Rev Geophys. 2018;56:532–652.

Appendix. Summary of Experiments

Table A-1 Summary of experiments

Name	Wet density (g/cc)	Gravimetric water content (w)	Air volume fraction (α_a)	Impulse (N·s)
Clay 1	1.82	0.0968	0.2178	28.91
Clay 3	1.93	0.0947	0.1697	35.06
Clay 4	1.77	0.0903	0.2472	31.89
Clay 5	1.72	0.1154	0.2457	36.42
Clay 6	1.87	0.1128	0.1815	40.13
Clay 7	1.98	0.1101	0.1328	42.22
Clay 8	1.78	0.1196	0.2146	42.07
Clay 9	1.77	0.1495	0.1932	48.85
Clay 10	1.88	0.1482	0.1429	51.43
Clay 11	1.78	0.1459	0.1935	44.56
Clay 12	1.71	0.1514	0.2166	46.35
Clay 13	1.64	0.1477	0.2534	38.86
Clay 14	2.06	0.1016	0.1099	39.6
Clay 15	2.19	0.1426	0.0074	93.75
Clay 16	2.01	0.0803	0.1543	32.81
Clay 17	1.65	0.0805	0.3086	24.11
Clay 18	1.7	0.0744	0.2864	24.21
Clay 19	1.44	0.0819	0.3886	22.77
Clay 20	1.6	0.1143	0.3012	28.45
Clay 21	1.43	0.0799	0.3958	23.05
Clay 22	1.55	0.1469	0.2963	36.84
Clay 23	1.19	0.1451	0.4597	26.44
Clay 24	1.64	0.115	0.2806	31.14
Clay 25	1.33	0.1132	0.4149	25.13
Clay 26	1.55	0.1266	0.3237	29.38
Clay 27	2.1	0.1254	0.0654	64.71
Clay 28	1.53	0.1195	0.3234	29.3
Clay 31	2.11	0.1153	0.0745	54.11
Clay 32	2.06	0.1157	0.0982	54.05
Clay 33	2.06	0.1169	0.0911	54.22
Clay 34	2.05	0.118	0.094	47.2
Clay 35	1.98	0.1173	0.1297	46.74
Clay 36	2.1	0.1145	0.0809	53.98
Clay 37	1.8	0.1201	0.2039	35.93
Clay 39	2.11	0.152	0.0367	82.62
Clay 40	1.35	0.1494	0.3819	28.8
Clay 41	1.97	0.155	0.1	63.6
Clay 42	2.22	0.0869	0.059	39.9
Clay 43	2.2	0.0937	0.0591	43.52
Clay 45	1.68	0.0002	0.3707	18.54
Clay 46	1.78	0.0108	0.3199	18.25
Clay 47	1.4	0.0096	0.468	14.77

Table A-1 Summary of experiments (continued)

Name	Wet density (g/cc)	Gravimetric water content (w)	Air volume fraction (α_a)	Impulse (N·s)
Clay 48	1.63	0.0106	0.3807	18.12
Clay 49	1.56	0.0047	0.4097	17.24
Clay 58	1.98	0.153	0.0957	61.87
Clay 59	1.88	0.1488	0.1426	48.2
Clay 60	1.93	0.1546	0.1146	61.06
Air Blast 50	NA	NA	1	6.68
Air Blast 51	NA	NA	1	6.11
Air Blast 52	NA	NA	1	6.51

Definitions of Soil State and Other Parameters

ρ - Wet or bulk density, the density of the material as tested (g/cm^3)

ρ_d - Dry density, density of the material after all the water has been removed (g/cm^3)

ρ_w - Density of water (g/cm^3)

G_s - Specific gravity, soil solid (mineral) density divided by water density; ratio of a given mass of soil solids at 23 °C to the same volume of deionized water at the same temperature.

w - Water content, ratio of water mass divided by soil solid mass

e - Void ratio, ratio of void volume to soil solid volume

φ - Porosity, ratio of void volume to total volume

I_a - Impulse on a target due to air blast

I_w - Impulse on a target from a charge shallowly buried in water

I_b - Impulse on a target due to a buried charge

I_r - Impulse ratio, $\frac{I_b}{I_a}$

a_a - Air-volume fraction, amount of the mixture that is air by volume

$$\boldsymbol{a_a = 1 - \frac{\rho_d}{\rho_w}\left(\frac{1}{G_s} - w\right)} \quad \text{(A-1)}$$

a_s - Soil-solids-volume fraction, amount of the mixture that is soil solids by volume

$$\boldsymbol{a_s = \left(\frac{\rho_d}{\rho_w G_s}\right)} \quad \text{(A-2)}$$

a_w - Water-volume fraction, amount of the mixture that is water by volume, also called volumetric water content

$$\boldsymbol{a_w = \left(\frac{\rho_d w}{\rho_w}\right)} \quad \text{(A-3)}$$

a_{sw} - Soil solids and water-volume content.

$$\boldsymbol{a_{sw} = 1 - a_a = \left(\frac{\rho_d}{\rho_w}\right)\left(\frac{1}{G_s} - w\right) = \frac{a_s}{\rho_w}(1 + wG_s)} \quad \text{(A-4)}$$

S - Saturation, the ratio of water volume to void volume

$$\boldsymbol{S = \frac{wG_s}{e}} \quad \text{(A-5)}$$

List of Symbols, Abbreviations, and Acronyms

CL	Red Lean Clay
CST	compaction sensitivity threshold
HMX	octogen
LL	liquid limit
LOS	line of saturation
ModP	modified Proctor
OPT	optimum moisture and density
PETN	pentaerythritol tetranitrate
PL	plastic limit
S	saturation
StdP; SP	standard Proctor
SSE	sum of squared errors
TNT	trinitrotoluene
USPS	Unified Soil Classification System

1 (PDF) DEFENSE TECHNICAL INFORMATION CTR DTIC OCA

1 (PDF) DEVCOM ARL FCDD RLD DCI TECH LIB

10 (PDF) DEVCOM ARL FCDD RLW TG
N GNIAZDOWSKI
E FIORAVANTE
S KUKUCK
S TROMBETTA
C CUMMINS
S HUG
D ABELL
J PRITCHETT
C R PECORA
D M FOX